Thermal-based modeling of coupled carbon, water and energy fluxes using nominal light use efficiencies constrained by leaf chlorophyll observations

Mitchell A. Schull[1], Martha C. Anderson[1], Rasmus Houborg[2], Anatoly Gitelson[3] and William P. Kustas[1]

[1] (USDA-ARS Hydrology and Remote Sensing Laboratory, Beltsville, MD, USA)

[2] (King Abdullah University of Science and Technology, Water Desalination and Reuse Center, Kingdom of Saudi Arabia)

[3] (Center for Advanced Land Management Information Technology (CALMIT), School of Natural Resources, University of Nebraska-Lincoln, Lincoln, NE, USA and Israeli Institute of Technology, Israel)

Correspondence to: M.A. Schull (mitchell.schull@ars.usda.gov)

Abstract

Recent studies have shown that estimates of leaf chlorophyll content (Chl), defined as the combined mass of chlorophyll a and chlorophyll b per unit leaf area, can be useful for constraining estimates of canopy light-use-efficiency (LUE). Canopy LUE describes the amount of carbon assimilated by a vegetative canopy for a given amount of Absorbed Photosynthetically Active Radiation (APAR) and is a key parameter for modeling land-surface carbon fluxes. A carbon-enabled version of the remote sensing-based Two-Source Energy Balance (TSEB) model simulates coupled canopy transpiration and carbon assimilation using an analytical sub-model of canopy resistance constrained by inputs of nominal LUE (β_n), which is modulated within the model in response to varying conditions in light, humidity, ambient CO_2 concentration and temperature. Soil moisture constraints on water and carbon exchange are conveyed to the TSEB-LUE indirectly through thermal infrared measurements of land-surface temperature. We investigate the capability of using Chl estimates for capturing seasonal trends in the canopy β_n from in situ measurements of Chl acquired in irrigated and rain-fed fields of soybean and maize near Mead, Nebraska. The results show that field-measured Chl is non-linearly related to β_n, with variability primarily related to phenological changes during early growth and senescence. Utilizing seasonally varying β_n inputs based on an empirical relationship with in-situ measured Chl resulted in improvements in carbon flux estimates from the TSEB model, while adjusting the partitioning of total water loss between plant transpiration and soil evaporation. The observed Chl-β_n relationship provides a functional mechanism for integrating remotely sensed Chl into the TSEB model, with the potential for improved mapping of coupled carbon, water, and energy fluxes across vegetated landscapes.

1. Introduction

The terrestrial biosphere continues to be impacted by climate change and increasing atmospheric carbon dioxide concentrations. Understanding the implications of these changes requires a thorough investigation of the patterns of terrestrial vegetation productivity and its feedback to global biogeochemical cycles of nitrogen and carbon. Vegetation productivity is defined as the production of organic matter by plants through photosynthesis. The total amount of organic matter produced via photosynthesis is known as gross photosynthesis. The total amount of CO_2 "fixed" by plants through photosynthesis over a spatial area for a unit time is termed gross primary productivity (GPP) (Gough, 2012).

Numerous micrometeorological studies have focused on measuring the net carbon flux between the atmosphere and land surface, also known as the net ecosystem carbon dioxide exchange (NEE). Field campaigns have been conducted around the world and in many different ecosystems, often employing the eddy covariance technique to provide information on seasonal and interannual variations in NEE (Baldocchi, 2003). Many studies estimate GPP from eddy-covariance observations of NEE and estimates of daytime ecosystem (soil + plant) respiration (Re) as GPP = NEE+Re (Suyker & Verma, 2010, 2012). Here, carbon uptake by plants is defined as positive while respiration, or carbon release, is negative.

Vegetation productivity is largely modulated by the amount of incoming radiation that is intercepted by plants. Many GPP and NEE modeling techniques are based on Monteith's hypothesis that the increase in canopy biomass is linearly related to the amount of light intercepted or absorbed by healthy, unstressed plants (Monteith, 1977). The slope of this relationship is known as the light use efficiency (LUE) or the conversion efficiency of light into

biomass through photosynthesis. Many LUE-based models have used fixed values of LUE derived from studies reported in the literature, assigned based on vegetation class (Anderson, Norman, Meyers, & Diak, 2000; Gower, Kucharik, & Norman, 1999). This practice is based on findings that maximum LUE tends to be relatively conservative within broad categories of plant functional type (Field, 1991; S J Goetz & Prince, 1999; Monteith, 1977).

Recent studies, however, have recognized that a more detailed spatio-temporal representation of LUE is needed to accurately determine the seasonal trends and magnitudes of carbon assimilation rates (Alton, North, & Los, 2007; DeLucia, Drake, Thomas, & Gonzalez-Meler, 2007; Houborg, Anderson, & Daughtry, 2009; Kosugi, Shibata, & Kobashi, 2003; Wilson, Baldocchi, & Hanson, 2001; Xu & Baldocchi, 2003). LUE can vary considerably within vegetation types, at different phenological stages and under varying environmental conditions that induce plant stress (Gower et al., 1999; Houborg, Anderson, Daughtry, Kustas, & Rodell, 2011; Houborg, Cescatti, Migliavacca, & Kustas, 2013; Medlyn, 1998; Prince, 1991; Ruimy, Kergoat, Bondeau, & intercomparison, 1999; Xu & Baldocchi, 2003). An analysis conducted by Kergoat et al. (2008) also supports the view that LUE varies significantly across and within biomes as well as among plant functional types. These studies highlight the need to account for variations in LUE due to plant phenological stage as well as changing conditions of light, humidity, and limited water and nutrient resources.

The challenge for regional-scale carbon flux mapping using a LUE-based modeling system is to find a parsimonious yet robust means for specifying LUE spatially across the modeling domain for different landcover types, and seasonally in response to changing phenology and plant stress conditions. Chlorophyll pigments absorb photosynthetically active radiation (PAR) and constitute a vital element in the photosynthetic machinery. Leaf chlorophyll

95 is mechanistically linked to photosynthetic capacity (Houborg et al., 2013) through functional
96 relationships with leaf nitrogen (Evans, 1989; Schlemmer et al., 2013) and Rubisco (Sage &
97 Pearcy, 1987; Theobald, Mitchell, Parry, & Lawlor, 1998) that acts as a catalyst for carbon
98 fixation within the leaf chloroplasts. These strong correlations make leaf chlorophyll an
99 important control on vegetation productivity by serving as a proxy for the nominal efficiency of
100 leaves in using the absorbed light for photosynthesis. The effective LUE will fluctuate in
101 response to short-term changes in environmental conditions (e.g. temperature, humidity, wind
102 speed), whereas the impact of variations in leaf chlorophyll will be more gradual as vegetation
103 stresses are not immediately manifested in observations of leaf chlorophyll content (Houborg et
104 al., 2011).

105 Recent studies have shown that the variation in midday GPP can be accurately estimated
106 via measurements of canopy-scale chlorophyll (Gitelson et al., 2006, 2012; Suyker & Verma,
107 2010, 2012). Changes in canopy chlorophyll are recognized to be sensitive to vegetation stress,
108 crop phenology and photosynthetic functioning of the vegetation, (Gitelson, Viña, Ciganda,
109 Rundquist, & Arkebauer, 2005; Ustin, Smith, Jacquemoud, Verstraete, & Govaerts, 1999; Zarco-
110 Tejada, Miller, Mohammed, Noland, & Sampson, 2002) and therefore can be related to GPP.
111 Leaf and canopy chlorophyll have also been shown to be useful quantities for constraining the
112 nominal LUE (β_n), over the course of the growing season (Gitelson et al., 2006, 2012; Houborg
113 et al., 2011, 2013; Monteith, 1972, 1977; Peng, Gitelson, Keydan, Rundquist, & Moses, 2011;
114 Peng & Gitelson, 2012). Chlorophyll is a vital pigment in the photosynthetic apparatus and
115 advances in the retrieval of leaf and canopy chlorophyll from remote sensing data (Houborg et
116 al., 2014) makes it extremely amenable for the ultimate goal of mapping fluxes over larger areas.

117 Houborg et al. (2011) demonstrated the utility of using remotely sensed maps of leaf
118 chlorophyll (Chl), defined as the combined mass of chlorophyll *a* and chlorophyll *b* per unit leaf
119 area, generated with the REGularized canopy reFLECtance (REGFLEC) inversion system
120 (Houborg & Anderson, 2009; Houborg et al., 2014) for constraining nominal LUE inputs.
121 REGFLEC-derived maps of β_n generated over a rain-fed maize production system at the
122 Beltsville Agricultural Research Center (BARC), MD were used as input to a version of the
123 thermal infrared (TIR) remote sensing based Two-Source Energy Balance Model (Anderson et
124 al., 2008; Houborg et al., 2011), which employs an analytical LUE-based model of canopy
125 resistance to compute coupled canopy transpiration and carbon assimilation fluxes (Anderson et
126 al., 2000). Soil moisture constraints on canopy resistance are effectively conveyed to the TSEB-
127 LUE by thermal infrared measurements of land-surface temperature (LST), incorporated via
128 principles of energy balance. Input values of β_n are modified internally within the model in
129 response to diurnally varying conditions in light, humidity, ambient CO_2 concentration and
130 temperature, and inferred soil water status. Houborg et al. (2011) found that REGFLEC derived
131 Chl was exponentially related to nominal LUE for drought conditions in 2007. The results
132 improved when a 3-day lag between Chl and β_n was imposed, suggesting that environmental
133 stresses were not immediately manifested in the measured Chl. Use of a seasonally varying β_n,
134 retrieved as a function of Chl, improved estimates of canopy carbon assimilation as well as latent
135 and sensible heat fluxes in comparison to runs using conventional fixed values of β_n derived
136 from the literature.
137 Here we extend the investigation of functional relationships between Chl and β_n using an
138 extensive dataset of in situ measurement of Chl collected fields of both irrigated and rain-fed
139 maize and soybean in Mead, NE. An empirically derived functional form of Chl versus

nominal β_n is used to drive the TSEB-LUE model at these sites using in-situ measurements of LST, Chl and micrometeorological variables, and model performance is evaluated using flux data from eddy covariance towers situated within the fields. A follow-on study will incorporate the TSEB-LUE into a multi-scale regional energy balance modeling system (Anderson, Kustas, & Norman, 2007) using β_n fields retrieved from remotely sensed estimates of Chl, enabling routine mapping of coupled carbon, water and energy fluxes at field to regional scales while taking into account critical spatio-temporal variations in photosynthetic capacities.

2. Model description

2.1. TSEB

The Two-Source (soil+canopy) Energy Balance (TSEB) model (Norman, Kustas, & Humes, 1995) is a thermal-based diagnostic flux model that couples micrometeorological conditions inside and above the canopy to energy fluxes from the soil, plants and atmosphere (Fig 1). The TSEB land surface model and refinements (Kustas & Norman, 1999, 2000) has been implemented within the Atmosphere-Land Exchange Inverse (ALEXI) regional modeling system, and the associated DisALEXI flux disaggregation approach (Anderson et al., 2007). The ALEXI-DisALEXI modeling paradigm facilitates flux mapping at continental to field scales through a combination of thermal infrared (TIR) imagery from geostationary and polar orbiting sensors (Anderson et al., 2011). The research in this paper, focusing on a local application of the TSEB approach using tower-based inputs, will be used to further refine regional remote sensing based flux mapping applications using ALEXI-DisALEXI.

The modeling system described here uses the series version of the TSEB (Kustas & Norman, 2000), which partitions available energy at the surface into sensible and latent heat

fluxes. The fluxes are computed separately for soil (subscript 's') and canopy (subscript 'c') components of the TIR measurement footprint:

$$(RN_c + RN_s) - G = (H_c + H_s) + (LE_c + LE_s) \quad (1)$$

The soil and canopy components of the net radiation ($RN_c;\ RN_s$) are modeled using equations found in (Kustas & Norman, 1999), while G is computed as a time-dependent fraction of RN_s (Santanello & Friedl, 2003). The model partitions remotely sensed LST (T_{rad}), observed at a view angle θ, into canopy and soil temperature components as,

$$T_{rad}(\theta) = [f_\theta T_c^4 + (1 - f_\theta) T_s^4]^{1/4} \quad . \quad (2)$$

Here f_θ is the fraction of vegetation cover as apparent from the TIR sensor view angle:

$$f_\theta = 1 - \exp\left(\frac{-0.5\Omega_\theta LAI}{cos\theta}\right) \quad (3)$$

where LAI is the Leaf Area Index (m^2/m^2) and Ω_θ is an angular dependent vegetation-clumping factor. Sensible heat flux from the soil (H_s) and canopy (H_c) and combined system (H) are then computed from the partitioned temperatures of canopy (T_c) and soil (T_s) using a temperature gradient series resistance network connecting the soil, canopy and atmosphere:

$$H_c = \rho c_p \frac{T_c - T_{AC}}{R_X} \quad (4)$$

$$H_s = \rho c_p \frac{T_s - T_{AC}}{R_S} \quad (5)$$

$$H = \rho c_p \frac{T_{AC} - T_A}{R_A} \quad (6)$$

Where R_X is the total two-sided leaf boundary resistance, R_s is the soil boundary resistance, and R_A is the aerodynamic resistance. The upper boundary condition in air temperature, T_A, is measured or estimated at a reference height above the canopy, while T_{AC} is a model-diagnosed in-canopy temperature. In the original form of the TSEB (referred to here as TSEB-PT), LE_c is computed using a modified Priestley-Taylor (PT) approach (Norman et al., 1995) applied to the

184 divergence of net radiation within the canopy. Soil evaporation, $LE_{s,}$ is calculated as a residual in
185 the energy balance equations. Negative LE_s values obtained at midday, indicating condensation
186 onto the soil, are considered non-physical and likely result from an overestimation of LE_c by the
187 PT approximation. This may occur under conditions of vegetation stress, where the rate of
188 transpiration is reduced from the potential PT estimate due to stomatal closure. In such
189 conditions the PT coefficient is iteratively reduced until LE_s approaches zero (Kustas, Norman,
190 Schmugge, & Anderson, 2004) .

191 *2.2. Analytical canopy resistance submodel (TSEB-LUE)*

192 Anderson et al. (2008) replaced the PT approximation for LE_c in TSEB-PT with an estimate of
193 canopy transpiration generated using an analytical LUE-based model of canopy resistance
194 (Anderson et al., 2000), enabling simulation of carbon fluxes in addition to energy and water
195 fluxes to the atmosphere. In comparison with TSEB-PT, TSEB-LUE requires additional
196 atmospheric inputs of ambient vapor pressure and CO_2 concentration, which serve as the upper
197 boundary for flux-gradient calculations of LE_c and A_c. It also requires specification of β_n, the
198 LUE expected under nominal unstressed conditions.
199 The system of equations and computational strategy used in TSEB-LUE are described in full in
200 Anderson et al. (2008). In brief, in TSEB-LUE LE_c and A_c are both defined using gradient-
201 resistance equations as shown in Fig. 1, coupled through simulated values of bulk canopy
202 resistance (R_c). Energy balance constraints on LE_c (informed by the T_c component of the
203 remotely sensed LST input) and LUE constraints on A_c (informed by the β_n input, typically
204 assigned by land-cover class) are used in combination to solve for R_c, as well as water vapor and
205 carbon concentrations inside the leaf and canopy. The bulk leaf boundary layer resistance (R_b)
206 and aerodynamic resistance (R_A) in Fig. 1 are dependent on wind speed and stability conditions,

as described in (Anderson et al., 2000). Here R_b, the canopy integrated two-sided leaf boundary layer resistance, is related to R_X, the total two-sided leaf boundary resistance as $R_b = (f_s/[f_g \times f_{dry}])R_X$, where f_s is distribution of stomata over the top and bottom of the leaf, f_g is the fraction of green vegetation and f_{dry} excludes the fraction of stomata that are blocked by leaf surface water. For a more detailed illustration of the coupled nature of the LE_c and A_c the reader is directed to eqs. A13 and A14 in the appendix of Anderson et al. (2008). Here we can see that the fluxes of LE_c and A_c are governed by R_c.

The LUE constraints on A_c are imposed as

$$A_c = \beta(\gamma) * APAR \quad (7)$$

where β is the effective LUE and γ is the ratio of intercellular (C_i) to ambient (C_a) CO_2 concentrations as diagnosed by the model and APAR is the absorbed photosynthetically active radiation . Under unstressed conditions we assume that the canopy will operate near β_n and a nominal value of C_i/C_a (γ_n). While curvilinear at the scale of individual leaves, the relationship between A_c and C_i has been shown to be more linearized at the canopy scale (Norman & Arkebauer, 1991). Therefore the deviation of effective LUE from the nominal value is estimated through the linear relationship

$$\beta(\gamma) = \frac{\beta_n}{\gamma_n - \gamma_0}(\gamma - \gamma_0) \quad (8)$$

where γ_0 is the value of γ when β is zero.

Anderson et al. (2008) determined that deviations of effective LUE from the nominal value $\Delta\beta = \beta_n - \beta$, generated by the TSEB-LUE, reflect both variability in ambient meteorological conditions and surface moisture conditions implied by the thermal signal. For example, riparian areas where soil moisture was non-limiting showed minimal $\Delta\beta$, while in areas with dense vegetation but relatively high T_c (in comparison with values expected for well-

230 watered vegetation), β was depressed more significantly from the nominally assigned value.
231 This indicates that the TIR inputs were conveying useful information regarding moisture
232 limitations on both canopy resistance and effective LUE – without the need of precipitation input
233 data and a detailed soil water balance characterization.

234 The study by Anderson et al. (2008) assumed that the nominal LUE is constant in time
235 for a given plant functional type. However, numerous studies cited above, including seasonal
236 tests with TSEB-LUE (Houborg et al., 2011), have demonstrated that the nominal value of LUE
237 can vary seasonally based on stand phenology and the canopy's changing capacity to fix carbon.
238 Here we investigate the ability of measurements of leaf chlorophyll content in maize and
239 soybean to accurately reflect seasonal changes in the β_n required by TSEB-LUE throughout
240 several growing seasons and under different water management strategies.

241 **3. Materials and methods**

242 *3.1. Study site*

243 This study uses data collected between 2002 and 2005 at the University of Nebraska-
244 Lincoln Agriculture and Development Center as part of the ongoing Carbon Sequestration
245 program. The research facility is located about 58 km northeast of Lincoln, NE, USA and
246 consists of 3 ~65 ha fields of maize (Zea mays, L) and soybean (Glycine max [L.] Merr.) (Fig.
247 2). Table 1 summarizes crop and water management by field for 2002-2005. Field 1 was
248 planted with continuous maize throughout the study period, while Fields 2 and 3 supported a
249 maize/soybean rotation cropping system. Fields 1 and 2 are equipped with a center pivot
250 irrigation system, while Field 3 relies entirely on rainfall. All three fields were managed in no-
251 till from 2001 through the extent of the study period examined here. Additional details regarding
252 long-term crop management and measurement activities at these field sites are provided in

253 Suyker et al. (2010).

254 *3.2.Micrometeorological observations*

255 An eddy covariance (EC) system has been deployed in each field, collecting continuous
256 measurements of latent heat (*LE*), sensible heat (*H*), CO_2 (*NEE*) and momentum fluxes. These
257 fluxes are routinely reported and available to the public as part of the AmeriFlux program.
258 Details regarding the flux and supporting micrometeorological instrumentation at Mead are
259 described in Suyker et al. (2010). In order to ensure the flux footprint/source area originated
260 essentially from the field encompassing the flux tower, the eddy covariance sensors were
261 mounted at 3 m above the ground for plant canopies that were shorter than 1 meter and were
262 moved to 6.2 m as the plant canopies grew for the remainder of each growing season.

263 Ancillary micrometeorological measurements were collected routinely on a separate
264 tower near each flux tower. The additional measurements include incident direct and diffuse
265 photosynthetically active radiation, with absorbed PAR (APAR) quantified using point and line
266 quantum sensors above and below the canopy. Air temperature and humidity were measured at 3
267 and 6 m above ground level, and radiation at 5.5 m. Multiple in- and between-row
268 measurements of soil heat flux at 0.06 m depth were combined to approximate an average flux.
269 Soil heat flux (G) values used here were corrected for heat storage above the plates.

270 EC fluxes computed for half hour intervals were assessed for closure of the energy
271 budget by comparing *LE+H* and *RN+G* during the study period. The regression slopes over the
272 study period ranged from 0.9 to 1 indicating generally reasonable closure. For comparison with
273 model results, energy closure was enforced by modifying the observed sensible and latent heat
274 fluxes such that the observed Bowen ratio was maintained (Twine et al., 2000).

3.3. Biophysical measurements

In order to facilitate research studies, biophysical data was collected continuously over the study period at six small plots (20 by 20 m) in each field. These plots, known as Intensive Measurement Zones (IMZ), were established such that they represent all major occurrences of soil and crop production zones within each field (Gitelson, Viña, et al., 2003; Viña, 2004). The collection of biophysical data within the IMZ areas is described in detail by [*Viña*, 2004] and only briefly reviewed here.

Within each IMZ, average leaf area per plant was estimated for both live and dead leaves using destructive samples collected every 10-14 days and measured using a LI-3100 area meter (LI-COR, INC., Lincoln, NE, USA). The total (LAI) and green leaf area (LAIg) was calculated as the leaf area per plant multiplied by the plant density (plants/m^2) at each IMZ. The LAI samples collected at the six IMZs were area-weighted averaged to obtain field-wide representative values (Gitelson et al., 2006).

The canopy clumping factor, Ω, used in Eq. 3, was empirically estimated for each site by optimizing the radiation scheme in TSEB-LUE, such that modeled midday APAR values matched observed values. Optimized Ω on non-clear days (fraction of direct radiation (fdir) < 80%) were removed and a linear interpolation between clear day values was applied. The allowed range in retrieved clumping factor ranged between 0.6 and 1.0.

In addition to LAI, reflectance measurements of the upper canopy leaves were taken every 2 weeks using an Ocean Optics USB2000 radiometer (400-900 nm) equipped with a leaf clip (Gitelson et al., 2005; Viña, Gitelson, Nguy-Robertson, & Peng, 2011). The Chl content was estimated from the reflectance data using a non-destructive methodology (Ciganda, Gitelson, & Schepers, 2009; Gitelson, Gritz, & Merzlyak, 2003). The method utilizes

298 reflectance in the red edge (700-720 nm) and NIR (760-800 nm) regions to approximate total
299 Chl, where Chl = a x [($R_{NIR}/R_{red\ edge}$)-1] ($\mu g\ cm^{-2}$). The model coefficient a was calibrated
300 using total Chl extracted in the lab. The linear model allowed for estimates of Chl in the range of
301 1- 90 $\mu g\ cm^{-2}$ with a Root Mean Square Error (RMSE) below 6 $\mu g\ cm^{-2}$. In order to estimate
302 average leaf chlorophyll content within the plant stand, leaf level measurements of chlorophyll
303 were multiplied by the fraction of green leaves (f_g)

304 $$Chl = Chl_{live} * f_g \quad (9)$$

305 where f_g was computed as the ration of green (LAIg) to total LAI, LAIg/LAI.

306 *3.4. Soil respiration and canopy assimilation*

307 TSEB-LUE estimates net carbon assimilation by the canopy (A_c). To evaluate model
308 output, the EC measurements of NEE ($A = A_c$-A_s in Fig. 1) must be corrected using estimates of
309 the soil respiration flux, A_s. Soil respiration was measured at approximately 3-week intervals at
310 each field site using a portable gas exchange system. Along with each soil respiration
311 measurement, soil temperatures at 10 cm were recorded and gravimetric soil water content was
312 determined for a 0–10 cm soil sample and converted to volumetric water contents (θ_{10}) using
313 measured bulk densities.

314 In order to interpolate between sampling dates, the measured soil respiration fluxes were
315 fit to an empirical equation (Norman, Garcia, & Verma, 1992) describing A_s as a function of soil
316 temperature (T_s), soil moisture and LAI:

317 $$A_s = (\mathrm{a} + \mathrm{bLAI})\theta_{10}\exp\left[\mathrm{c}\left(T_{s,10} - 25.0\right)\right] \quad (10)$$

318 where θ_{10} is the soil moisture content in the 0-10 cm depth, $T_{s,10}$ is the temperature of the soil at

319 a depth of 10 cm and the site-specific regression coefficients a, b, and c were derived empirically
320 every year for each field. The hourly canopy carbon assimilation (A_c) was then obtained by
321 adding estimates of hourly soil respiration (A_s), derived from hourly in-field observations of θ_{10}
322 and $T_{s,10}$ along with daily interpolated LAI, to net ecosystem exchange (A) (sign convention used
323 here is such that A_c and A_s are positive away from the surface).

324 *3.5. Nominal LUE optimization*

325 The seasonal variation in model input values of β_n were determined at five-day intervals
326 for each field and study year by minimizing differences between measured and modeled canopy
327 CO_2 fluxes (A_c). The TSEB-LUE model was run for all three fields using tower measurements of
328 incident solar radiation, incoming longwave radiation, air temperature, wind speed, atmospheric
329 pressure and vapor pressure as well as outgoing longwave radiation. The measured outgoing
330 longwave radiation was inverted using the Stefan-Boltzmann law to estimate half-hourly LST
331 (T_{RAD}). Previous studies (S. J. Goetz, Halthore, Hall, & Markham, 1995; Hatfield, Vauclin,
332 Vieira, & Bernard, 1984) have indicated that this provides a more representative measurement of
333 the composite (soil+vegetation) surface temperature than do measurements from infrared
334 thermometers, which have relatively narrow field of view. These runs used leaf and canopy
335 parameters for maize and soybean tabulated in Houborg et al. (2009), and field-average estimates
336 of LAI (section 3.3) linearly interpolated to daily values over the study period.

337 Following Houborg et al. (2011), the optimization process varied β_n over a prescribed
338 range, selecting daily values that minimized bias between modeled and measured Ac fluxes
339 during daytime hours (constrained to solar zenith angles (SZA) less than 50 degrees).
340 Optimized values of β_n were then averaged over 5-day periods. Only clear days were

341 considered, defined such that the fraction of direct radiation was greater than 50%. LUE is
342 known to increase under more diffuse lighting conditions because light is more uniformly
343 distributed over the canopy (Norman & Arkebauer, 1991). By constraining to clear days, the
344 resulting optimized β_n are relevant to future remote sensing applications, which require clear-sky
345 conditions for direct retrieval of TIR-based LST and a gap-filling algorithm for estimating fluxes
346 during cloudy periods. In addition, we considered fluxes only over medium to dense vegetation
347 (LAI>2) where Ac dominates the observed system CO2 flux and β_n optimization is well-
348 constrained. The end product was a time-series of 5-day averaged β_n determined over the
349 growing season for each year and site, optimized for use within the TSEB-LUE modeling
350 framework.

351 **4. Results and Discussion**

352 *4.1. Relationship between Chl and β_n*

353 Figure 3 shows examples of the time evolution of optimized nominal LUE and
354 measurements of Chl over the growing season obtained for representative irrigated soybean (a)
355 and maize (b) fields. There is a general correspondence between time trends in β_n and Chl, but
356 with some deviation particularly in the beginning of the season when LAI is low. At these times,
357 the canopy assimilation is small and optimization of β_n using measured *Ac* is not as reliable.
358 Therefore, in deriving empirical functional relationships between β_n and Chl we only consider
359 observations collected over medium to dense vegetation (LAI > 2) where canopy carbon
360 assimilation is significant. This does not imply, however, that the functional relationships
361 cannot be used over sparse vegetation. The results discussed in sections 4.2, 4.3 and tables 3 and
362 4 show results from sparse to dense vegetation.

363 Scatter plot comparisons of β_n and Chl for all sites and years are shown in Fig. 4,

364 discriminating maize from soybean and irrigated from rainfed fields. Nominal LUE is shown to
365 be non-linearly sensitive to Chl, and the reasonable goodness of fit (r^2=0.52) provides support for
366 the use of Chl as a remote sensing observable for retrieving β_n inputs to TSEB-LUE. While
367 separate functional relationships for soybean and maize were explored (not shown), the benefits
368 of employing these species-specific relationships did not outweigh the advantage of having a
369 single functional fit. A more elaborate dataset on soybean will be needed for further
370 investigations into functional differences in the Chl– β_n response between soybean and maize.
371 Figure 4 indicates that a single function can be used to describe the relationship for both crops,
372 despite the differences in photosynthetic pathway between soybean (C_3) and maize (C_4) crops.
373 While semi-mechanistic relationships between leaf chlorophyll content and leaf photosynthetic
374 capacity demonstrate the importance of distinguishing between species utilizing differing
375 photosynthetic pathways (C3 versus C4) (Houborg et al., 2013), relationships at the canopy scale
376 are governed by different mechanism sometimes yielding more universal relationships (Gitelson
377 et al., 2006). For soybean, assimilation rate begins to saturate at approximately 30 (μg cm^{-2}) Chl
378 corresponding to a β_n of 0.025 (Fig. 4). C_4 crops can assimilate more carbon per unit APAR by
379 maintaining the concentration of CO_2 at a high level in the leaf so that photorespiration is
380 minimized, and saturation occurs at a higher Chl (~60 μg cm^{-2}) and β_n (~0.035) value. These are
381 close to the conventional values of β_n found in the literature such as those used in the fixed β_n
382 studies of Anderson et al. (2008, 2000) and Houborg et al. (2009).

383 The functional fit for $\beta_n(Chl)$ plotted in Fig. 4 takes the form of β_n= a(1-exp(b*Chl))
384 and was composed using a customized nonlinear least squares fit. The approach finds the
385 regression coefficients that minimize the error between x (Chl) and y (β_n). Here the coefficients
386 *a* (95% confidence bounds) and *b* are 0.039 (0.038, 0.040) and 28.14 (26.18, 30.10) respectively

with a r^2 of 0.52. A leave-one-out cross validation reveals that β_n can be estimated from Chl with an RMSE of 0.0042 mol mol^{-1} for both maize and soybean.

Though it is evident that there is a considerable amount of deviation from the functional fit, there are some potential explanations for this deviation. The outliers that appear to have higher β_n values for low Chl values are predominantly rain-fed maize (Fig. 4). A lower planting density to maximize efficiency could explain these outliers. In fact, the rain-fed field 3 is planted at a lower density for both maize and soybean (Table 2). Lower plant density appears to have little affect on soybean likely due to the difference in plant structure. In maize a lower planting density allows deeper penetration of light into the canopy and an increase in the intensity of diffuse light, which can enhance effective LUE by up to 15 % in maize (Norman & Arkebauer, 1991). Another important factor may be the adopted multiplication of in-situ measured Chl with the fraction of green vegetation in order to produce an average (comprising both green and senescent leaf material) Chl over the canopy (Houborg et al., 2014). This assumes in-situ sampling of entirely green leaf material, which may result in underestimation of the actual Chl particularly during advanced stages of leaf senescence or vegetation stress. This is particularly evident in the rain-fed fields of maize as seen in Fig. 4.

4.2. Evaluation of hourly fluxes from TSEB-LUE

Seasonal variations in both total latent heat flux and carbon assimilation over representative fields of irrigated maize and soybean are shown in Fig. 5. Each diurnal segment is represented by flux measurements averaged by hour over 5-day intervals. The averaging scheme reduces the random errors associated with flux observations as well as natural variability for each time period (Moncrieff, Malhi, & Leuning, 1996). Statistical metrics comparing observed and

409 modeled fluxes at the hourly timestep are tabulated in Table 3, including Mean Bias Error
410 (MBE), Root Mean Square Difference (RMSD), coefficient of regression (r^2), coefficient of
411 efficiency (E), and percent error (%error). The statistics in table 3 are generated from a randomly
412 selected 2/3 of the dataset to test the robustness of the Chl - β_n functional fit.

413 The impact of including the seasonally varying nominal LUE (as a function of Chl) in the
414 TSEB-LUE is most evident in model estimates of carbon assimilation (Fig. 5a,b), with lesser
415 impact on total fluxes of latent (Fig. 5c,d) and sensible heat. Differences between simulated
416 carbon fluxes forced using a fixed β_n (red line) and a β_n dictated by variations in Chl (blue line)
417 are particularly pronounced for maize (Fig. 5a) especially during senescence. Statistical metrics
418 describing model performance at a hourly timestep (Table 3), demonstrate a significant decrease
419 in the RMSD from 9 to 5 μmol m^{-2} s^{-1} when adopting seasonally varying β_n (as a function of
420 Chl) rather than a fixed β_n. The coefficient of determination improves from 0.83 to 0.91, the
421 coefficient of efficiency increases from 0.68 to 0.90, and the relative error is reduced to 18%
422 using a varying β_n down from 28 % using a fixed β_n (Table 3). Clearly, by adopting fixed
423 literature-based β_n values designed for healthy vegetation, carbon assimilation may be
424 overestimated during times of vegetation stress and senescence and underestimated during times
425 of optimal plant health.

426 In this study, the impact on the total latent heat flux was minimal as evidenced by the
427 RMSD values of 51 and 52 W m^{-2} using seasonally fixed values of β_n and β_n(Chl), respectively
428 (Table 3). Impacts on sensible heat fluxes were similarly minimal. In contrast, Houborg et al.
429 (2011) noted a significant improvement in latent heat fluxes over maize during severe drought
430 conditions. The datasets used in the current analysis are based on collections over irrigated and
431 to a lesser extent rain-fed fields not significantly affected by drought conditions over the studied

period, and more research is still needed to reveal the impact of drought stress on β_n and latent heat fluxes.

While the impact of including the varying β_n on total (canopy+soil) latent heat fluxes is not immediately evident given the conditions sampled in this study period, there was a significant impact on the partitioning between canopy and soil latent heat (Fig. 6). In general, the predominant effect was to increase soil evaporation and decrease transpiration fluxes, indicating a shift of latent heat from the canopy to soil. Changes in the canopy latent heat fluxes are intimately (and positively) linked to changes in carbon assimilation through regulation via the canopy resistance (Anderson et al., 2008).

Scatter plot comparisons of modeled and measured hourly energy and carbon fluxes are shown in Figures 7 and 8, respectively. Incorporation of time-varying β_n serves to modulate the partition of the fluxes of carbon and water between the soil and canopy but it has little impact on the total energy fluxes in this study (Table 3). In contrast, the overall impact on the canopy carbon flux is more pronounced, with a significant reduction in bias and increased goodness of fit (Fig. 8 and Table 3).

4.3. Evaluation of daily-integrated fluxes

Daytime-integrated fluxes of water, energy and carbon were computed using the 5-day averaged hourly flux values integrated over daytime hours where the solar zenith angle is less than 80 degrees. Figure 9a shows the results of the daily fluxes forced by the fixed β_n. The latent heat fluxes are seen to be slightly overestimated at low to mid range values whereas the sensible heat fluxes are slightly underestimated at mid to high range values. The results based on seasonally varying β_n are quite similar (Fig. 9b), although the apparent overestimation of the latent heat fluxes seen in Fig. 9a has been slightly reduced. This improvement is reflected in the

455 RMSD statistic, which changes from 1.44 to 1.41 (Table 4).

456 The use of a seasonally varying β_n rather than a fixed β_n, markedly improves modeled
457 carbon fluxes at the daily time scale (Fig. 10). Errors at daily timesteps are significantly reduced
458 over hourly model performance, with decreases in RMSD and MBE from 0.60 to 0.32 and 0.47
459 to 0.14 μmol m^{-2} s^{-1}, respectively, and a decrease in relative error from 26% to 13% (Table 4).

460 **5. Summary and Conclusions**

461 The results presented in this study indicate that leaf chlorophyll (Chl) is closely related to the
462 canopy nominal light use efficiency (β_n) input required by TSEB-LUE for medium to dense
463 vegetation. In addition, the relationship can be reasonably described with a single function for
464 both soybean and maize, despite differences in photosynthetic pathway (C_3 versus C_4). The
465 relationship between Chl and β_n was found to be curvilinear with β_n saturating for soybean
466 around a value of 0.025 corresponding to a Chl value of approximately 30 (μg/cm^2) while maize
467 appears to saturate at a β_n value closer to 0.035 corresponding to a Chl level of around 60
468 (μg/cm^2). These asymptotic values are in line with literature values and previous applications
469 with the TSEB-LUE using fixed β_n.

470 During times of plant stress or senescence, the use of a fixed land cover specific nominal
471 LUE representative of healthy vegetation is not appropriate. By allowing nominal LUE to
472 respond to varying conditions of plant stress via Chl modulations, uncertainties in modeled
473 fluxes of carbon are significantly reduced. While canopy carbon assimilation shows improved
474 results especially in the senescing stage of the growing season, the impact is not apparent in total
475 latent heat fluxes. However varying β_n adjusts the partitioning of latent heat fluxes from the soil

476 and canopy. Unfortunately information about the partitioning of the fluxes was not available for
477 verification purposes.
478 The results indicate potential for improved monitoring of carbon fluxes using established
479 relationships as a functional basis for using Chl as a proxy of plant condition and photosynthetic
480 capacity. Because Chl can be estimated from remotely sensed data (Houborg & Anderson, 2009;
481 Houborg et al., 2014), the approach outlined in this paper can be scaled up using satellite data
482 with the potential for improved regional mapping of fluxes of carbon, water, and energy. For
483 regional scale mapping the challenge will be to establish the spatial distribution of species to
484 inform the model for different nominal values (i.e. γ_n), which can vary between C_3 to C_4 plants.
485 For agricultural areas the USDA's Cropland Data Layer (CDL) can be used; however, for other
486 biomes a more robust species map may be needed then currently exists. By implementing the
487 TSEB-LUE approach within the ALEXI/DisALEXI modeling system (Anderson et al., 2007),
488 regional scale modeling of not only water and energy but also carbon fluxes within a thermal-
489 based modeling framework will become feasible.
490
491
492
493
494
495
496
497
498

Acknowledgements

The research presented here was funded by NASA Headquarters under the Terrestrial Ecology (Grant NNH09ZDA001N) Program. We appreciate the data provided by the Center for Advanced Land Management Information Technologies (CALMIT) and the Carbon Sequestration Program, University of Nebraska-Lincoln.

522 **References**

523 Alton, P. B., North, P. R., & Los, S. O. (2007). The impact of diffuse sunlight on canopy light-
524 use efficiency, gross photosynthetic product and net ecosystem exchange in three forest
525 biomes. *Global Change Biology*, *13*(4), 776–787.

526 Anderson, M. C., Kustas, W. P., & Norman, J. M. (2007). Upscaling Flux Observations from
527 Local to Continental Scales Using Thermal Remote Sensing. *Agronomy Journal*, *99*(1),
528 240–254.

529 Anderson, M. C., Kustas, W. P., Norman, J. M., Hain, C., Mecikalski, J. R., Schultz, L., … Gao,
530 F. (2011). Mapping daily evapotranspiration at field to continental scales using
531 geostationary and polar orbiting satellite imagery. *Hydrology And Earth System Sciences*,
532 *15*(1), 223–239.

533 Anderson, M. C., Norman, J. M., Kustas, W. P., Houborg, R., Starks, P. J., & Agam, N. (2008).
534 A thermal-based remote sensing technique for routine mapping of land-surface carbon,
535 water and energy fluxes from field to regional scales. *Remote Sensing Of Environment*,
536 *112*(12), 4227–4241.

537 Anderson, M. C., Norman, J. M., Meyers, T. P., & Diak, G. R. (2000). An analytical model for
538 estimating canopy transpiration and carbon assimilation fluxes based on canopy light-use
539 efficiency . *Agricultural And Forest Meteorology*, *101*, 265–289.

540 Baldocchi, D. D. (2003). Assessing the eddy covariance technique for evaluating carbon dioxide
541 exchange rates of ecosystems: past, present and future. *Global Change Biology*, *9*(4), 479–
542 492.

543 Ciganda, V. S., Gitelson, A. A., & Schepers, J. (2009). Non-destructive determination of maize
544 leaf and canopy chlorophyll content. *Journal of Plant Physiology*, *166*(2), 157–167.

545 DeLucia, E. H., Drake, J. E., Thomas, R. B., & Gonzalez-Meler, M. (2007). Forest carbon use
546 efficiency: is respiration a constant fraction of gross primary production? *Global Change*
547 *Biology*, *13*(6), 1157–1167.

548 Evans, J. R. (1989). Photosynthesis and nitrogen relationships in leaves of C3 plants. *Oecologia*,
549 *78*(1), 9–19.

550 Field, C. B. (1991). Ecological scaling of carbon gain to stress and resource availability BT -
551 Response of Plants to Multiple Stresses. In H. A. Moony, W. E. Winner, & E. J. Pell (Eds.),
552 *Response of Plants to Multiple Stresses* (pp. 35–65). San Diego: Academic Press.

553 Gitelson, A. A., Gritz, Y., & Merzlyak, M. N. (2003). Relationships between leaf chlorophyll
554 content and spectral reflectance and algorithms for non-destructive chlorophyll assessment
555 in higher plant leaves. *Journal of Plant Physiology*, *160*(3), 271–282.

556 Gitelson, A. A., Peng, Y., Masek, J. G., Rundquist, D. C., Verma, S. B., Suyker, A. E., …
557 Meyers, T. P. (2012). Remote estimation of crop gross primary production with Landsat
558 data. *Remote Sensing Of Environment*, *121*, 404–414.

559 Gitelson, A. A., Viña, A., Arkebauer, T. J., Rundquist, D. C., Keydan, G., & Leavitt, B. (2003).
560 Remote estimation of leaf area index and green leaf biomass in maize canopies.
561 *Geophysical Research Letters*, *30*(5), 1248.

562 Gitelson, A. A., Viña, A., Ciganda, V. S., Rundquist, D. C., & Arkebauer, T. J. (2005). Remote
563 estimation of canopy chlorophyll content in crops. *Geophysical Research Letters*, *32*(8),
564 L08403.

565 Gitelson, A. A., Viña, A., Verma, S. B., Rundquist, D. C., Arkebauer, T. J., Keydan, G., …
566 Suyker, A. E. (2006). Relationship between gross primary production and chlorophyll
567 content in crops: Implications for the synoptic monitoring of vegetation productivity.
568 *Journal Of Geophysical Research-Atmospheres*, *111*(D).

569 Goetz, S. J., Halthore, R. N., Hall, F. G., & Markham, B. L. (1995). Surface temperature retrieval
570 in a temperate grassland with multiresolution sensors. *Journal of Geophysical Research*,
571 *100*(D12), 25397. doi:10.1029/94JD02684

572 Goetz, S. J., & Prince, S. D. (1999). Modelling Terrestrial Carbon Exchange and Storage:
573 Evidence and Implications of Functional Convergence in Light-use Efficiency BT -
574 Advances in ecological research. In A. H. Fitter & D. Raffaelli (Eds.), *Advances in*
575 *ecological research* (Vol. 28, pp. 57–92). San Diego: Academic Press.

576 Gough, C. M. (2012). Terrestrial Primary Production: Fuel for Life. *Nature Education*
577 *Knowledge*, *3*(10), 28.

578 Gower, S. T., Kucharik, C. J., & Norman, J. M. (1999). Direct and Indirect Estimation of Leaf
579 Area Index, fAPAR, and Net Primary Production of Terrestrial Ecosystems. *Remote*
580 *Sensing Of Environment*, *70*(1), 29–51.

581 Hatfield, J. L., Vauclin, M., Vieira, S. R., & Bernard, R. (1984). Surface temperature variability
582 patterns within irrigated fields. *Agriculture Water Management*, *8*, 429–437.

583 Houborg, R., & Anderson, M. C. (2009). Utility of an image-based canopy reflectance modeling
584 tool for remote estimation of LAI and leaf chlorophyll content at regional scales. *Journal Of*
585 *Applied Remote Sensing*, *3*(1), 3529.

586 Houborg, R., Anderson, M. C., & Daughtry, C. S. T. (2009). Utility of an image-based canopy
587 reflectance modeling tool for remote estimation of LAI and leaf chlorophyll content at the
588 field scale. *Remote Sensing Of Environment*, *113*(1), 259–274.

589 Houborg, R., Anderson, M. C., Daughtry, C. S. T., Kustas, W. P., & Rodell, M. (2011). Using
590 leaf chlorophyll to parameterize light-use-efficiency within a thermal-based carbon, water
591 and energy exchange model. *Remote Sensing Of Environment*, *115*(7), 1694–1705.

592 Houborg, R., Cescatti, A., Migliavacca, M., & Kustas, W. P. (2013). Satellite retrievals of leaf
593 chlorophyll and photosynthetic capacity for improved modeling of GPP. *Agricultural And*
594 *Forest Meteorology*, *177*, 10–23.

595 Houborg, R., McCabe, M. F., Cescatti, A., Gao, F., Schull, M., & Gitelson, A. A. (2014). Joint
596 leaf chlorophyll content and leaf area index retrieval from Landsat data using a regularized
597 model inversion system. *Submitted to Remote Sensing of Environment*.

598 Kergoat, L., Lafont, S., Arneth, A., Le Dantec, V., & Saugier, B. (2008). Nitrogen controls plant
599 canopy light-use efficiency in temperate and boreal ecosystems. *Journal of Geophysical*
600 *Research: Biogeosciences*, *113*(G), 4017.

601 Kosugi, Y., Shibata, S., & Kobashi, S. (2003). Parameterization of the CO2 and H2O gas
602 exchange of several temperate deciduous broad‐leaved trees at the leaf scale considering
603 seasonal changes. *Plant, Cell and Environment*, *26*(2), 285–301.

604 Kustas, W. P., & Norman, J. M. (1999). Evaluation of soil and vegetation heat flux predictions
605 using a simple two-source model with radiometric temperatures for partial canopy cover.
606 *Agricultural And Forest Meteorology*, *94*(1), 13–29.

607 Kustas, W. P., & Norman, J. M. (2000). A two-source energy balance approach using directional
608 radiometric temperature observations for sparse canopy covered surfaces. *Agronomy*
609 *Journal*, *92*(5), 847–854.

610 Kustas, W. P., Norman, J. M., Schmugge, T. J., & Anderson, M. C. (2004). Mapping surface
611 energy fluxes with radiometric temperature. In D. A. Quattrochi & J. C. Luvall (Eds.),
612 *Thermal Remote Sensing in Land Surface Processes* (pp. 205–254). Boca Raton: CRC
613 Press.

614 Medlyn, B. E. (1998). Physiological basis of the light use efficiency model. *Tree Physiology*,
615 *18*(3), 167–176.

616 Moncrieff, J. B., Malhi, Y., & Leuning, R. (1996). The propagation of errors in long-term
617 measurements of land-atmosphere fluxes of carbon and water. *Global Change Biology*,
618 *2*(3), 231–240. doi:10.1111/j.1365-2486.1996.tb00075.x

619 Monteith, J. L. (1972). Solar radition and productivity in tropical ecosystems. *Journal Of Applied*
620 *Ecology*, *9*(3), 747–766.

621 Monteith, J. L. (1977). Climate and the Efficiency of Crop Production in Britain. *Philosophical*
622 *Transactions of the Royal Society of London. Series B*, *281*(9), 277–294.

623 Norman, J. M., & Arkebauer, T. J. (1991). Predicting Canopy Photosynthesis and Light-Use
624 Efficiency from Leaf Characteristics. In K. J. Boote & R. S. Loomis (Eds.), *Modeling Crop*
625 *Photosynthesis—from Biochemistry to Canopy* (pp. 75–94). Crop Science Society of
626 America and American Society of Agronomy.

627 Norman, J. M., Garcia, R., & Verma, S. B. (1992). Soil surface CO2 fluxes and the carbon
628 budget of a grassland. *Journal Of Geophysical Research-Atmospheres*, *97*(D), 18845.

629 Norman, J. M., Kustas, W. P., & Humes, K. S. (1995). Source Approach for Estimating Soil and
630 Vegetation Energy Fluxes in Observations of Directional Radiometric Surface-
631 Temperature. *Agricultural And Forest Meteorology*, *77*, 263–293.

632 Peng, Y., & Gitelson, A. A. (2012). Remote estimation of gross primary productivity in soybean
633 and maize based on total crop chlorophyll content. *Remote Sensing Of Environment*,
634 *117*(C), 440–448.

635 Peng, Y., Gitelson, A. A., Keydan, G., Rundquist, D. C., & Moses, W. (2011). Remote
636 estimation of gross primary production in maize and support for a new paradigm based on
637 total crop chlorophyll content. *Remote Sensing Of Environment*, *115*(4), 978–989.

638 Prince, S. D. (1991). A model of regional primary production for use with coarse resolution
639 satellite data. *International Journal Of Remote Sensing*, *12*, 1313–1330.

640 Ruimy, A., Kergoat, L., Bondeau, A., & intercomparison, T. participants of the P. N. P. P.
641 model. (1999). Comparing global models of terrestrial net primary productivity (NPP):
642 analysis of differences in light absorption and light-use efficiency. *Global Change Biology*,
643 *5*(S1), 56–64.

644 Sage, R. F., & Pearcy, R. W. (1987). The Nitrogen Use Efficiency of C3 and C4 Plants. *Plant*
645 *Physiology*, *84*, 959–963. doi:10.1104/pp.84.3.954

646 Santanello, J. A., & Friedl, M. A. (2003). Diurnal covariation in soil heat flux and net radiation.
647 *Journal of Applied Meteorology*, *42*(6), 851–862.

648 Schlemmer, M., Gitelson, A. A., Schepers, J., Ferguson, R., Peng, Y., Shanahan, J., &
649 Rundquist, D. (2013). Remote estimation of nitrogen and chlorophyll contents in maize at
650 leaf and canopy levels. *International Journal of Applied Earth Observation and*
651 *Geoinformation*, *25*, 47–54.

652 Suyker, A. E., & Verma, S. B. (2010). Coupling of carbon dioxide and water vapor exchanges of
653 irrigated and rainfed maize–soybean cropping systems and water productivity. *Agricultural*
654 *And Forest Meteorology*, *150*(4), 553–563.

655 Suyker, A. E., & Verma, S. B. (2012). Gross primary production and ecosystem respiration of
656 irrigated and rainfed maize–soybean cropping systems over 8 years. *Agricultural And*
657 *Forest Meteorology*.

Theobald, J. C., Mitchell, R. A. C., Parry, M. A. J., & Lawlor, D. W. (1998). Estimating the Excess Investment in Ribulose-1 , 5-Bisphosphate Carboxylase / Oxygenase in Leaves of Spring Wheat Grown under Elevated CO 21, 945–955.

Twine, T. E., Kustas, W. P., Norman, J. M., Cook, D. R., Houser, P. R., Meyers, T. P., … Wesely, M. L. (2000). Correcting eddy-covariance flux underestimates over a grassland. *Agricultural And Forest Meteorology*, *103*(3), 279–300.

Ustin, S. L., Smith, M. O., Jacquemoud, S., Verstraete, M., & Govaerts, Y. (1999). Geobotany: Vegetation Mapping for Earth Sciences BT - Manual of Remote Sensing, Remote Sensing for the Earth Sciences. In A. Rencz & R. Ryerson (Eds.), *Manual of Remote Sensing, Remote Sensing for the Earth Sciences* (Vol. 3). John Wiley & Sons.

Viña, A. (2004). *Remote Estimation of Leaf Area Index and Biomass in Corn and Soybean*. (A. A. Gitelson, Ed.). ProQuest Dissertations And Theses; Thesis (Ph.D.)--The University of Nebraska - Lincoln, The University of Nebraska - Lincoln.

Viña, A., Gitelson, A. A., Nguy-Robertson, A. L., & Peng, Y. (2011). Comparison of different vegetation indices for the remote assessment of green leaf area index of crops. *Remote Sensing Of Environment*, *115*(12), 3468–3478.

Wilson, K. B., Baldocchi, D. D., & Hanson, P. J. (2001). Leaf age affects the seasonal pattern of photosynthetic capacityand net ecosystem exchange of carbon in a deciduous forest. *Plant, Cell and Environment*, *24*(6), 571–583.

Xu, L., & Baldocchi, D. D. (2003). Seasonal trends in photosynthetic parameters and stomatal conductance of blue oak (Quercus douglasii) under prolonged summer drought and high temperature. *Tree Physiology*, *23*(13), 865–877.

Zarco-Tejada, P. J., Miller, J. R., Mohammed, G. H., Noland, T. L., & Sampson, P. H. (2002). Vegetation stress detection through chlorophyll a+b estimation and fluorescence effects on hyperspectral imagery. In *Journal of Environmental Quality* (Vol. 31, pp. 1433–1441). York Univ, Ctr Res Earth & Space Sci, Toronto, ON M3J 1PE, Canada.

691 **Table 1.** Cropping and water management history at Mead study field sites.

Year	2002	2003	2004	2005
Field 1	Irrigated corn	Irrigated corn	Irrigated corn	Irrigated corn
Field 2	Irrigated soybean	Irrigated corn	Irrigated soybean	Irrigated corn
Field 3	Rain-fed soybean	Rain-fed corn	NA	Rain-fed corn

692

693 **Table 2.** Planting density (Plants/m^2)

Year	2002	2003	2004	2005
Field 1	7.1	7.7	8.0	6.9
Field 2	33.3	7.8	29.6	7.6
Field 3	30.5	5.7	NA	5.4

694

695 **Table 3.** Statistical metrics for hourly measured and modeled fluxes using 2/3 of the fields/years
696 for validation. Energy flux units are W $m^{-2}$and carbon flux units are μmol $m^{-2}s^{-1}$

Flux	*N*	O	MBE	RMSD	r^2	*E*	*% error*
Fixed							
RN	1680	347	6	29	0.89	0.98	5
LE	1680	268	0	51	0.84	0.90	14
H	1680	43	-4	35	0.68	0.76	62
G	1680	41	7	23	0.68	0.73	42
Ac	1680	23	5	9	0.83	0.68	28
f(Chl)							
RN	1680	347	5	29	0.88	0.98	5
LE	1680	269	-5	52	0.82	0.90	14
H	1680	45	0	35	0.67	0.77	59
G	1680	40	7	22	0.70	0.75	42
Ac	1680	23	2	5	0.91	0.90	18

697 [a] Here N is the number of observations, O is the mean observed flux, RMSD is the root-mean-square difference
698 between the modeled (P) and observed (O) values, MBE is the mean bias error (P − O), r^2 is the coefficient of
699 determination for the linear regression of P on O, E is the coefficient of efficiency, and the percent error is defined
700 as the mean absolute difference between P and O divided by the mean observed flux.
701
702
703
704
705
706
707
708
709
710
711
712
713
714

715 **Table 4.** Statistical metrics comparing daily measured and modeled fluxes using 2/3 of the
716 fields/years for validation. Energy flux units are MJ $m^{-2}d^{-1}$and carbon flux units are
717 gC $m^{-2}d^{-1}$

Flux	*N*	O	MBE	RMSD	r^2	*E*	*% error*
Fixed							
RN	140	14	0.21	0.76	0.97	0.96	4
LE	140	11	0.18	1.44	0.89	0.89	10
H	140	2	-0.08	1.07	0.76	0.74	50
G	140	2	0.23	0.58	0.77	0.66	25
Ac	140	2	0.47	0.60	0.91	0.64	26
f(Chl)							
RN	140	14	0.1	0.74	0.97	0.96	4
LE	140	11	-0.16	1.41	0.88	0.88	10
H	140	2	0.07	1.03	0.78	0.76	55
G	140	2	0.29	0.61	0.77	0.65	27
Ac	140	2	0.14	0.32	0.92	0.90	13

718
719
720
721
722
723
724
725
726
727
728
729
730
731

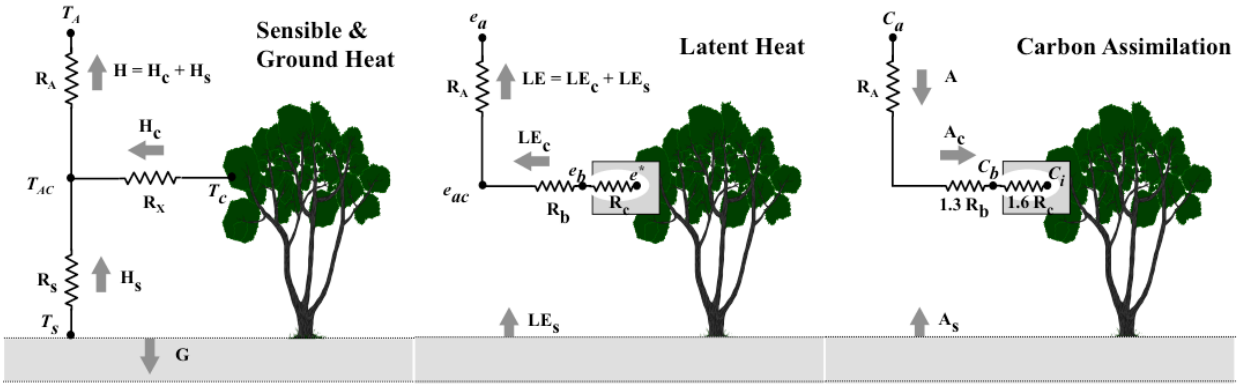

Fig. 1. Schematic illustrating the LUE-based canopy resistance method, diagramming its role within TSEB framework for computing coupled carbon, water and energy fluxes.

Fig. 2. Location of the irrigated (lower left) and rain-fed (upper right) study fields. The white dots represent the locations of the micrometeorological towers.

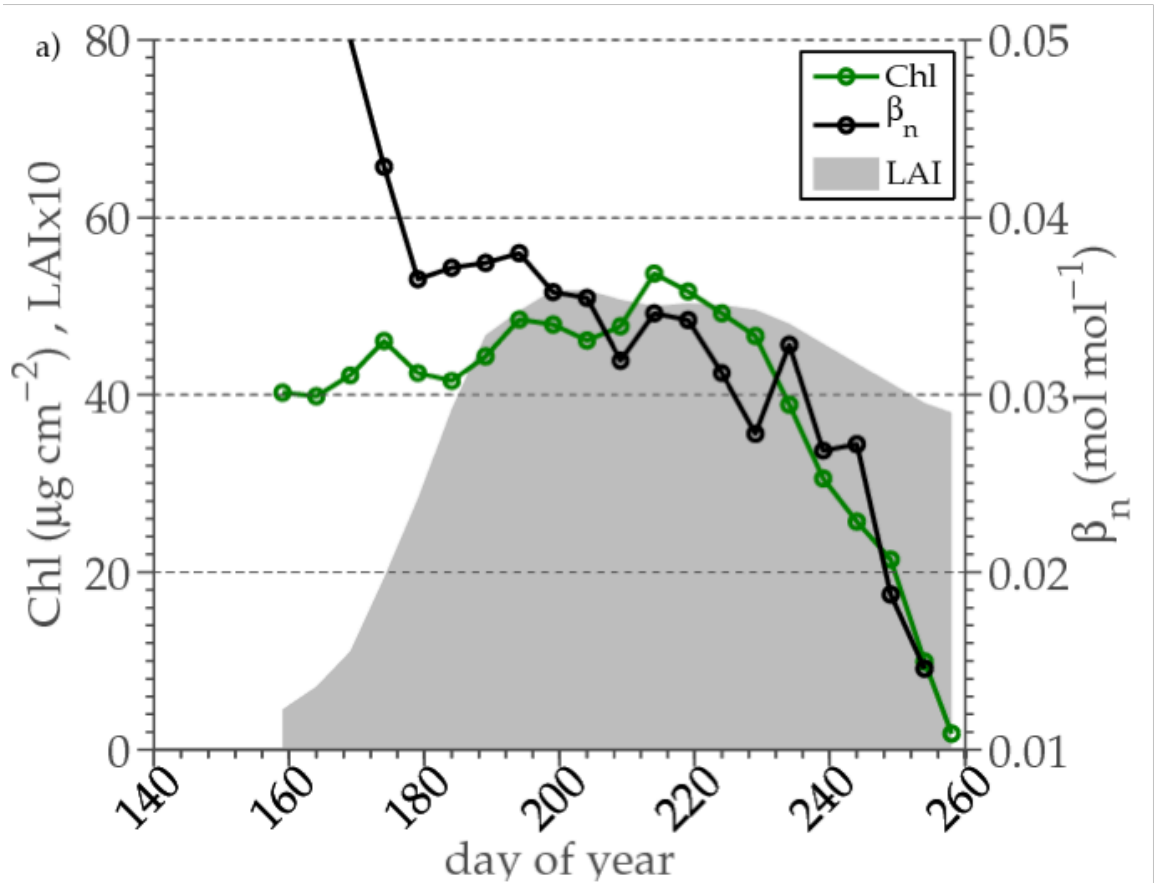
a)
Chl
β_n
LAI
Chl (µg cm^{-2}) , LAIx10
β_n (mol mol^{-1})
day of year
0
20
40
60
80
0.01
0.02
0.03
0.04
0.05
140
160
180
200
220
240
260

744
745

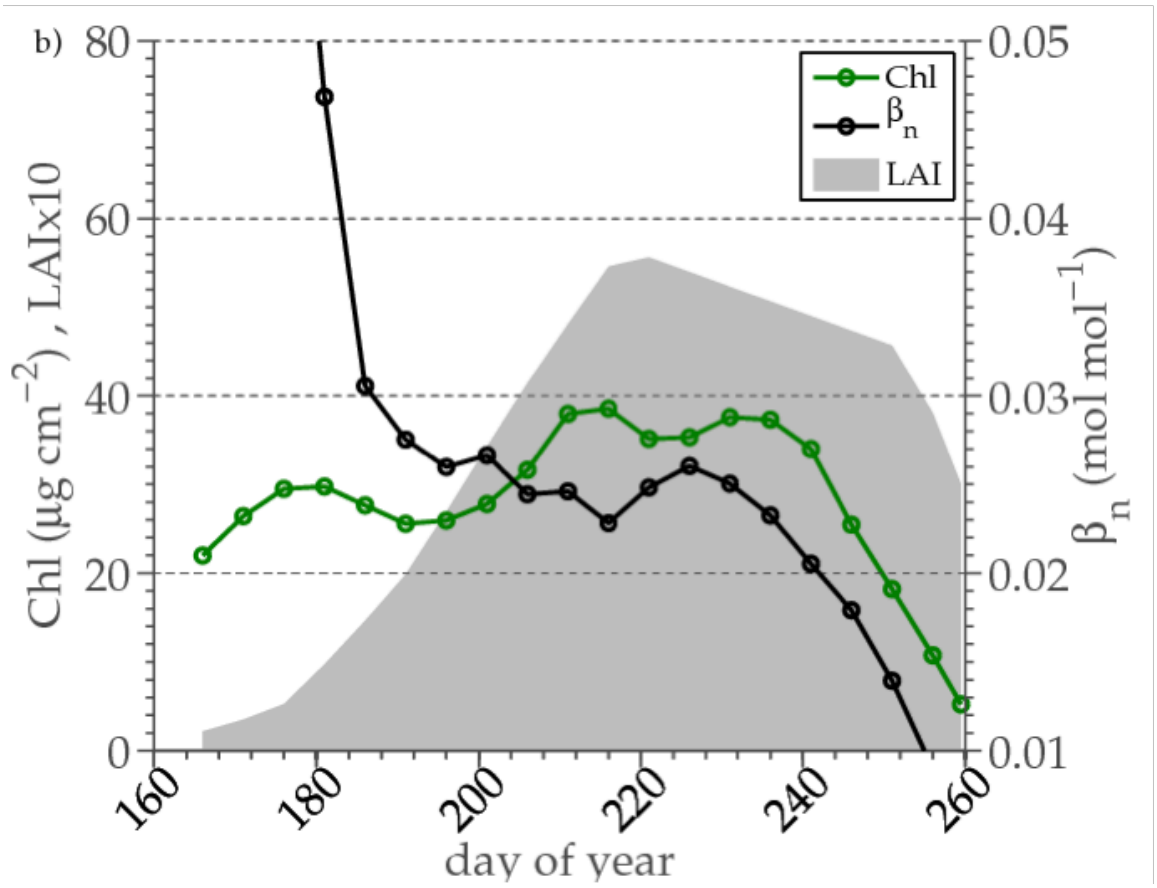

Fig. 3. Seasonal trends of β_n, leaf Chl and LAI for a) an irrigated maize field (field 1, 2005), b) an irrigated soybean field (field 2, 2002)

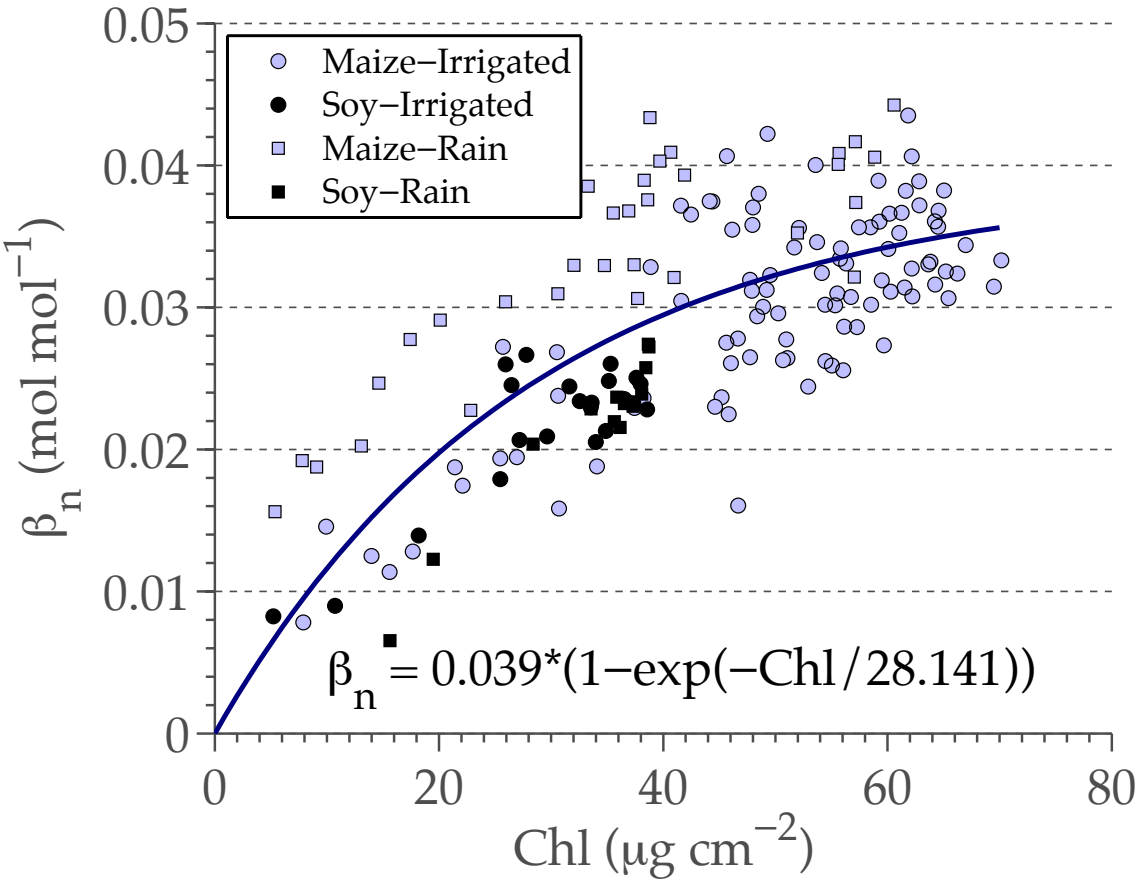

Fig. 4. Functional relationship derived between Chl and β_n for irrigated and rain-fed fields of maize and soybean.

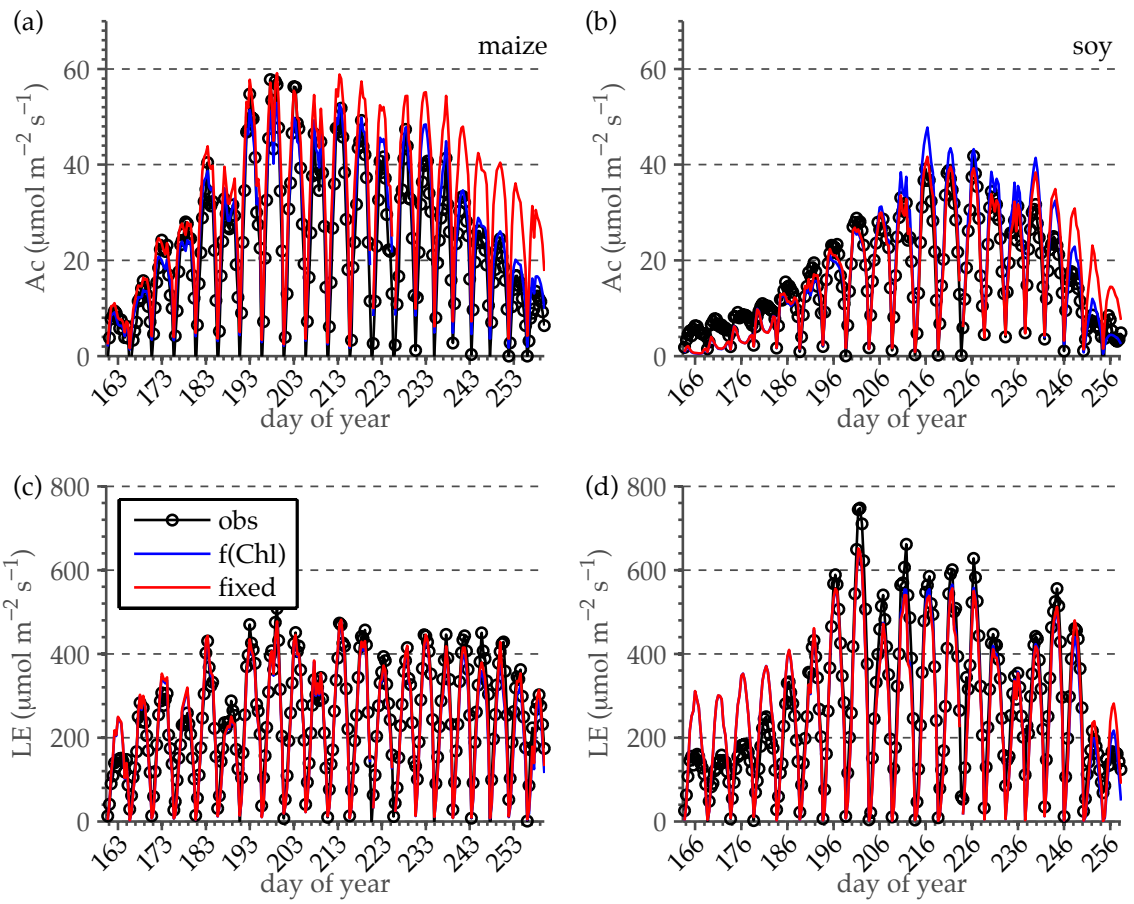

Fig. 5. Seasonal variations in hourly canopy fluxes of carbon and latent heat over maize (left panels: field 1, 2004) and soybean (right panels: field 2, 2002). Fluxes modeled using fixed β_n are shown in red and fluxes modeled using β_n as a function of Chl are shown in blue. Each diurnal period shown represent fluxes averaged hourly over a 5-day segment.

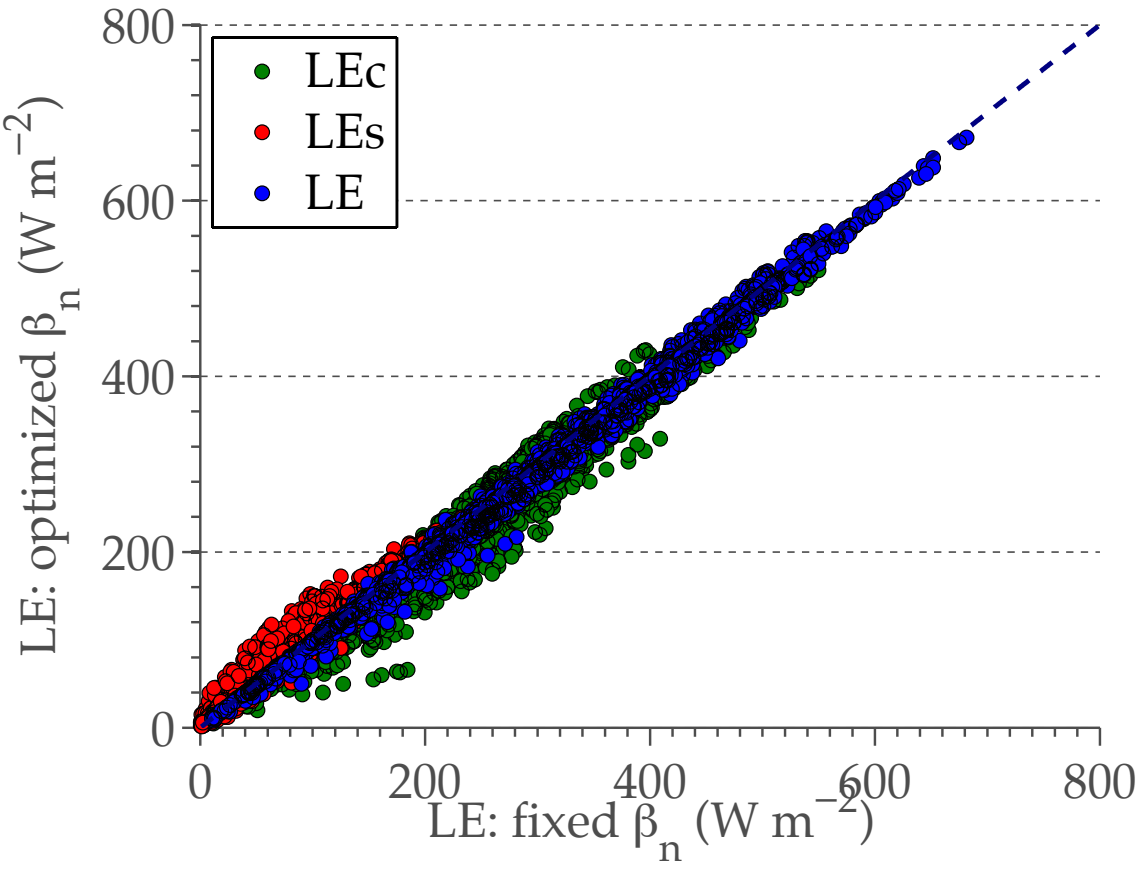

Fig. 6. Comparison of hourly TSEB_LUE estimates of latent heat flux over maize and soybean field, generated using a fixed values β_n and using β_n as a function of Chl. The green circles are the latent heat fluxes from the canopy and red circles represent latent heat fluxes from the soil. The blue filled circles are the total (soil+canopy) latent heat fluxes.

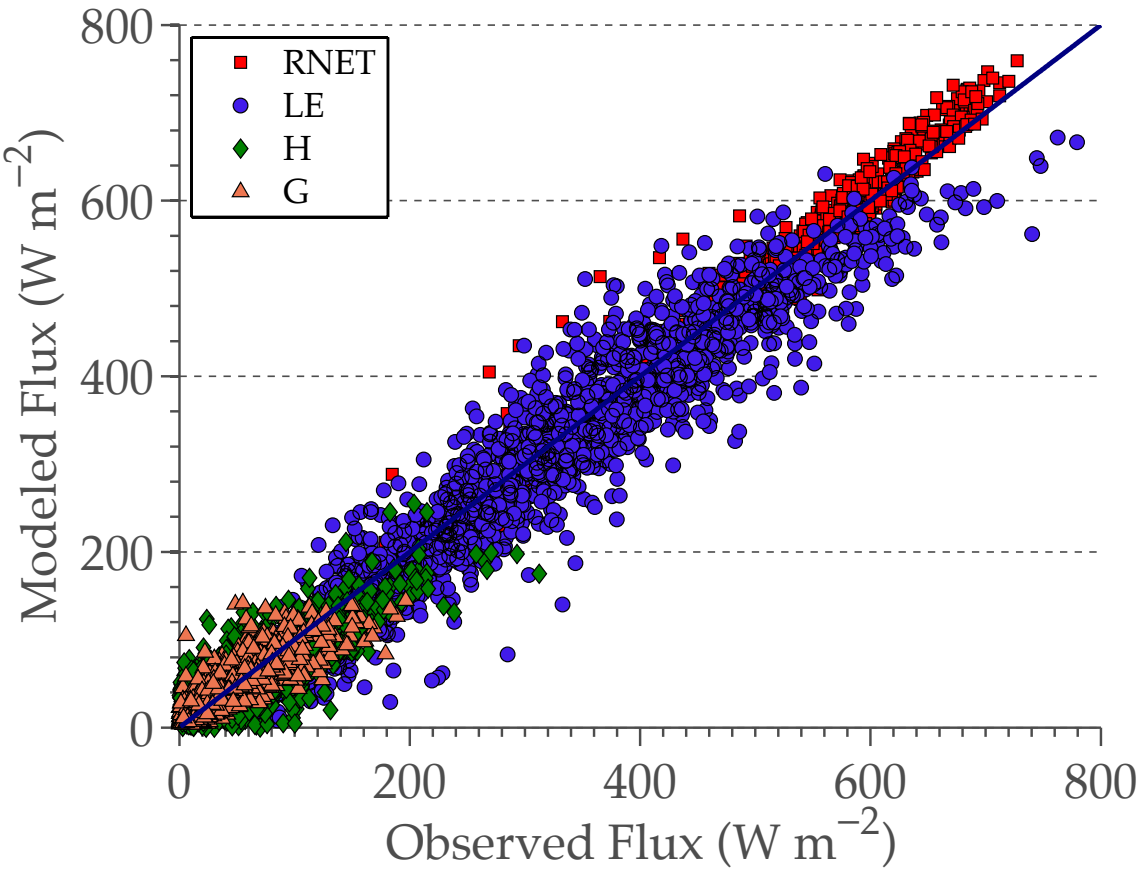

Fig. 7. Comparison of hourly modeled and measured energy balance components for maize and soybean at Mead, NE, generated with TSEB-LUE using β_n as a function of Chl.

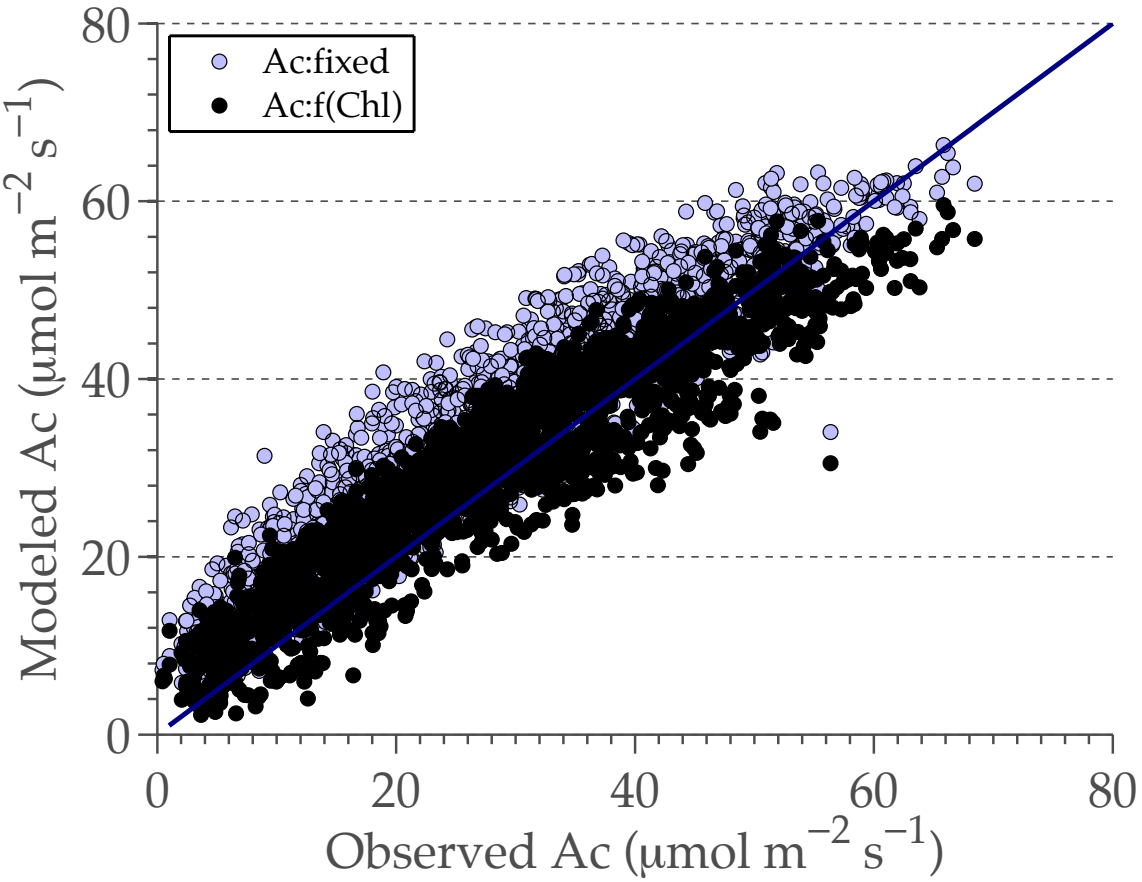

Fig. 8. Comparison of hourly modeled and measured energy balance components for maize and soybean at Mead, NE, generated with TSEB-LUE using fixed values of β_n (hollow points) and β_n as a function of Chl (solid points).

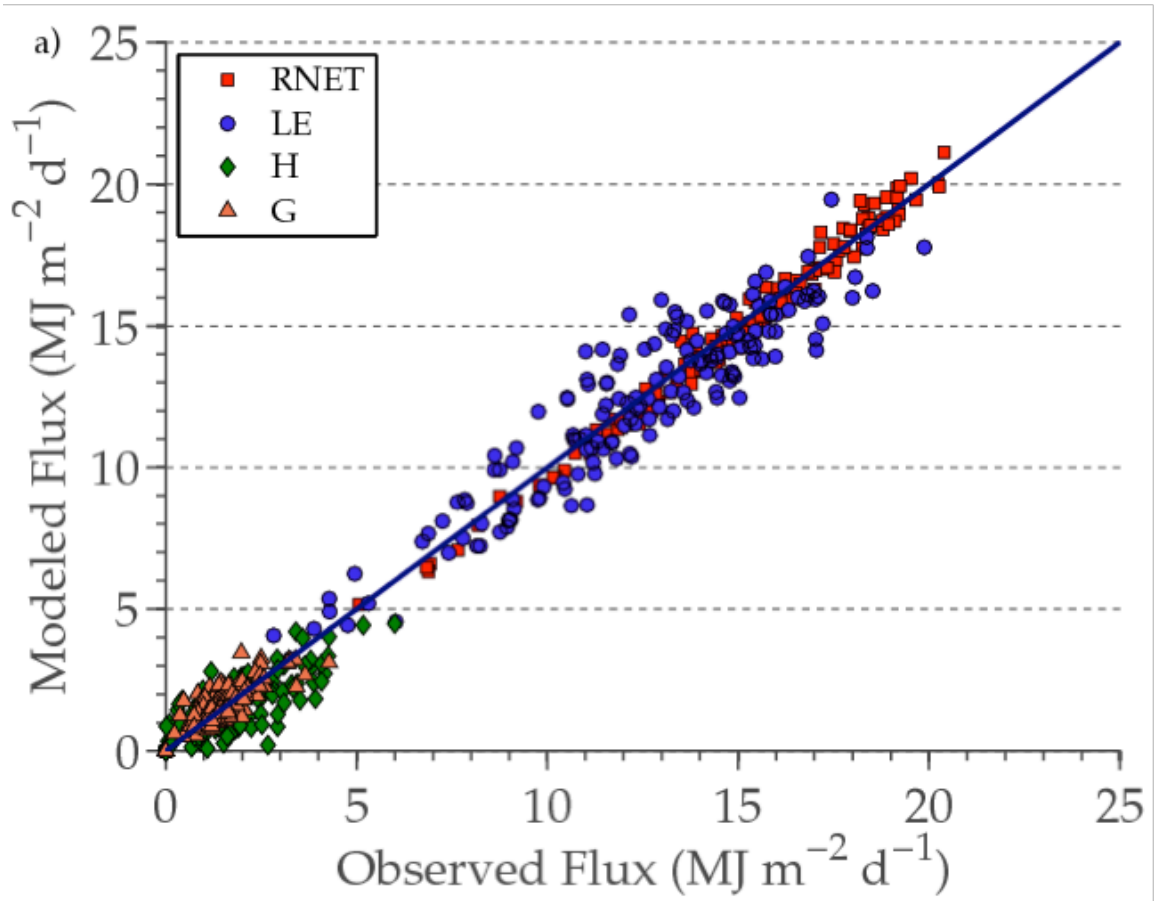
a)
RNET
LE
H
G
Modeled Flux (MJ m^{-2} d^{-1})
Observed Flux (MJ m^{-2} d^{-1})
0
5
10
15
20
25

801
802

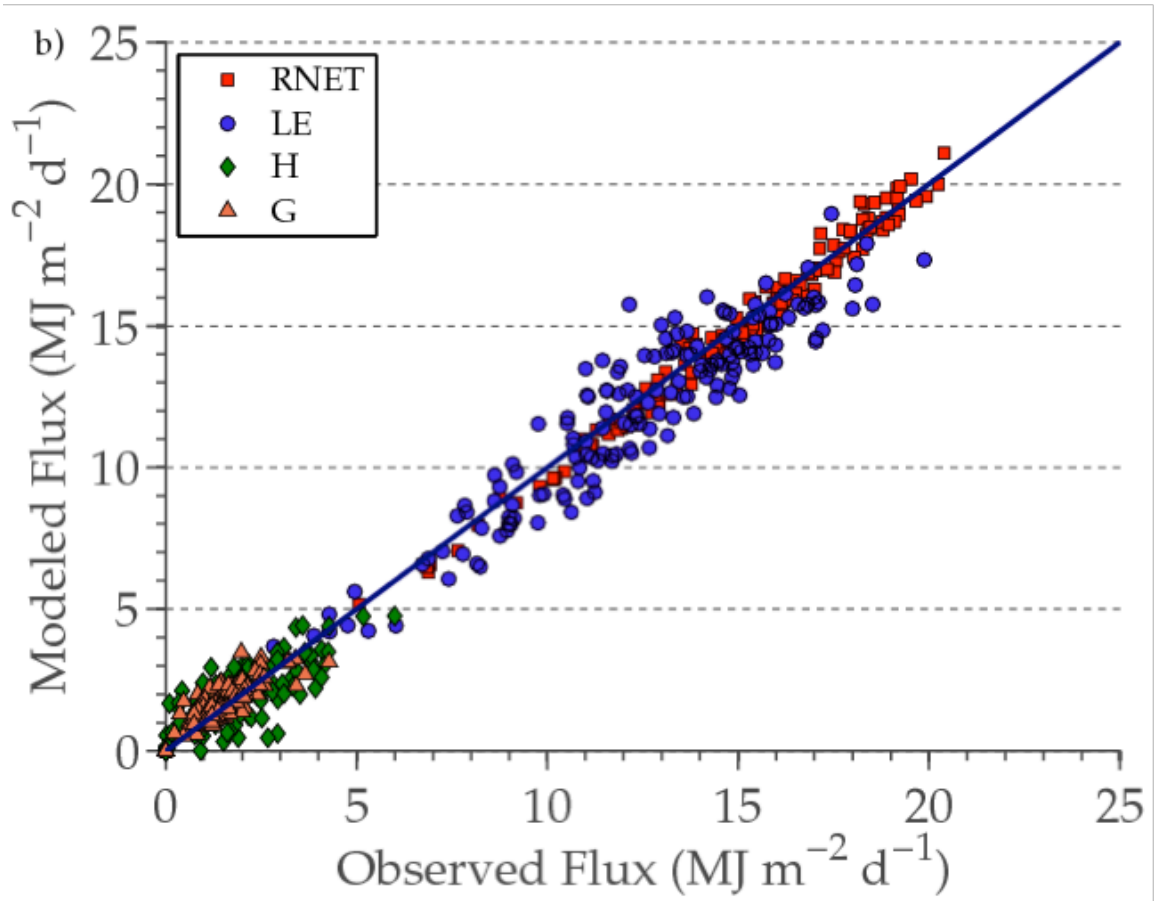

Fig. 9. Comparison of daily modeled and measured energy balance components for maize and soybean at Mead, NE using TSEB-LUE with a) fixed β_n and b) β_n as a function of Chl.

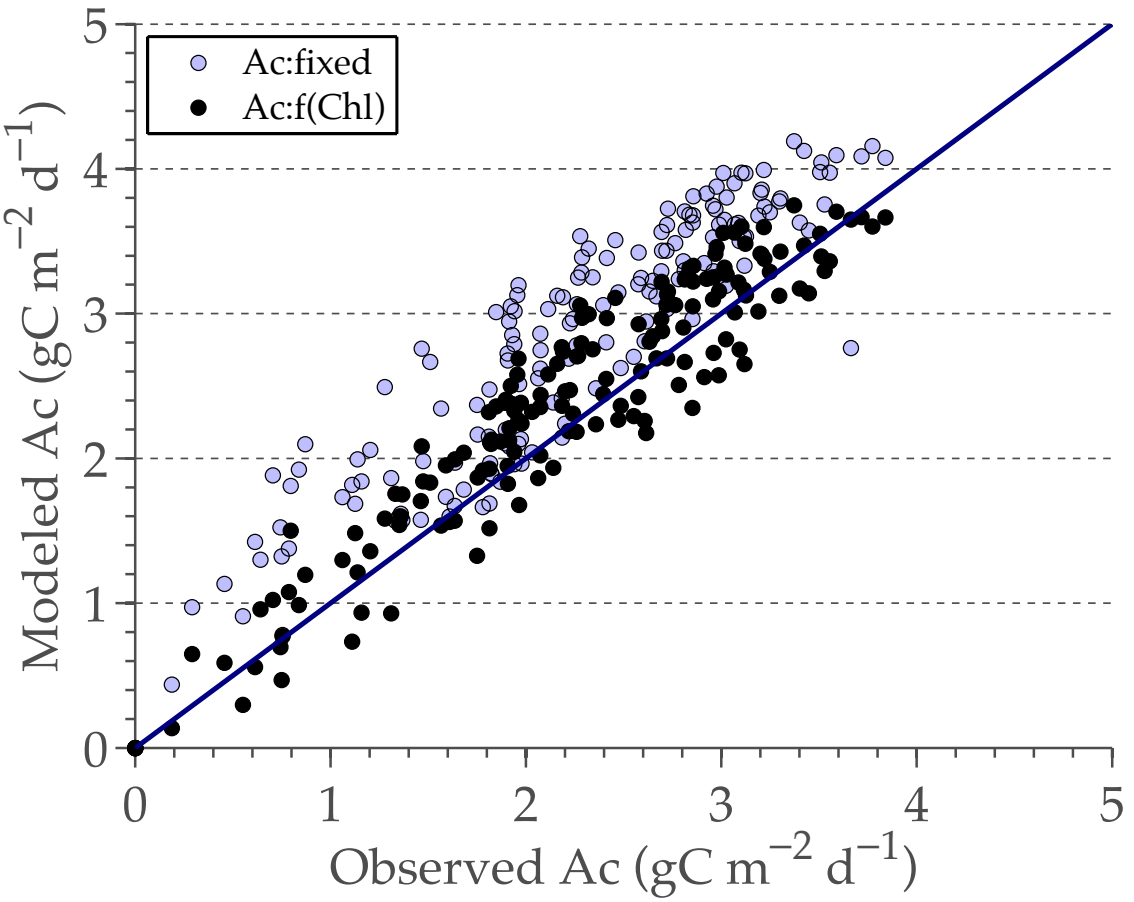

Fig. 10. Comparison of hourly modeled and measured canopy carbon assimilation fluxes for maize and soybean at Mead, NE, generated with TSEB-LUE using fixed values of β_n (hollow points) and β_n as a function of Chl (solid points).